Nuclear Engineering and Technology 50 (2018) 1138–1147

Contents lists available at ScienceDirect

Nuclear Engineering and Technology

journal homepage: www.elsevier.com/locate/net

Original Article

Theoretical models of threshold stress intensity factor and critical hydride length for delayed hydride cracking considering thermal stresses

Jingyu Zhang [a], Jiacheng Zhu [a], Shurong Ding [a, *], Liang Chen [b], Wenjie Li [b], Hua Pang [b]

[a] Institute of Mechanics and Computational Engineering, Department of Aeronautics and Astronautics, Fudan University, Shanghai 200433, China
[b] Science and Technology on Reactor System Design Technology Laboratory, Nuclear Power Institution of China, Chengdu 610041, Sichuan, China

ARTICLE INFO

Article history:
Received 24 May 2018
Received in revised form
29 June 2018
Accepted 6 July 2018
Available online 11 July 2018

Keywords:
Delayed hydride cracking
Threshold stress intensity factor
Critical hydride length
Zircaloy tubes
Radial cracking

ABSTRACT

Delayed hydride cracking (DHC) is an important failure mechanism for Zircaloy tubes in the demanding environment of nuclear reactors. The threshold stress intensity factor, K_{IH}, and critical hydride length, l_C, are important parameters to evaluate DHC. Theoretical models of them are developed for Zircaloy tubes undergoing non-homogenous temperature loading, with new stress distributions ahead of the crack tip and thermal stresses involved. A new stress distribution in the plastic zone ahead of the crack tip is proposed according to the fracture mechanics theory of second-order estimate of plastic zone size. The developed models with fewer fitting parameters are validated with the experimental results for K_{IH} and l_C. The research results for radial cracking cases indicate that a better agreement for K_{IH} can be achieved; the negative axial thermal stresses can lessen K_{IH} and enlarge the critical hydride length, so its effect should be considered in the safety evaluation and constraint design for fuel rods; the critical hydride length l_C changes slightly in a certain range of stress intensity factors, which interprets the phenomenon that the DHC velocity varies slowly in the steady crack growth stage. Besides, the sensitivity analysis of model parameters demonstrates that an increase in yield strength of zircaloy will result in a decrease in the critical hydride length l_C, and K_{IH} will firstly decrease and then have a trend to increase with the yield strength of Zircaloy; higher fracture strength of hydrided zircaloy will lead to very high values of threshold stress intensity factor and critical hydride length at higher temperatures, which might be the main mechanism of crack arrest for some Zircaloy materials.

1. Introduction

Owing to low neutron absorption cross-section and excellent pellet cladding interaction resistance [1], Zircaloy cladding tubes have been extensively used in boiling water reactors (BWRs) and pressurized water reactors (PWRs). Delayed hydride cracking (DHC) was reported to occur in the cladding tubes by detailed post irradiation examinations [2–4], where long and shallow axial cracks were found to initiate outside or inside the cladding tubes and propagate in the radial direction. This kind of radial failure mode has been a potential concern for guaranteeing the fuel cladding safety.

Generally, DHC is regarded as a repeated coupling process, including the stress-induced diffusion and accumulation of hydrogen atoms ahead of the stress concentrator, brittle hydride precipitation and fracture [1]. Cracking happens and gives rise to a new crack tip only after a period of waiting time to reach the critical hydride length, l_C. This subcritical crack-growth behavior only occurs when the actual stress intensity factor, K_I, is larger than the threshold stress intensity factor, K_{IH}, for Mode I cracking [5]. So, the threshold stress intensity factor and critical hydride length are important parameters to evaluate the safety of Zircaloy tubes.

A number of theoretical models [5–8] have been proposed for the threshold stress intensity factor and critical hydride length. Near the crack tip, there is usually a plastic zone which has a length, r_p along the cracking direction. The yield criterion is satisfied at the boundary of plastic zone with a normal stress σ_p, which is the stress component perpendicular to the crack plane.

Most models for K_{IH} are developed based on a fracture criterion that fracture occurs when the maximum normal stress

* Corresponding author.
E-mail addresses: dingshurong@fudan.edu.cn, dsr1971@163.com (S. Ding).

https://doi.org/10.1016/j.net.2018.07.001

perpendicular to the crack plane at a distance of r_M ahead of the crack tip reaches a critical value, and can be described as

$$\sigma(r_M) + \sigma^h(r_M) = \sigma_F \quad (1)$$

where $\sigma(r_M)$ is the maximum stress in the plastic zone induced by the external loads when there is no hydride present; r_M is the position where the maximum stress, $\sigma(r_M)$, exists; $\sigma^h(r_M)$ is the normal stress at r_M induced only by the formation of hydride; σ_F is the fracture strength of hydrided Zircaloy.

The critical hydride length l_C is also an important parameter to calculate the DHC velocity for a given stress intensity factor K_I. A model was developed by Shmakov et al. [5], where the critical hydride length l_C was dependent on K_{IH} and r_M. As mentioned above, the location of the maximum stress r_M plays an important role in determining K_{IH}, so it is of significance to obtain the value of r_M and the relation with the applied stress intensity factor.

One can realize that it is very important to determine the maximum stress $\sigma(r_M)$ and its location, which depend on the plastic zone size, r_p, and the normal stress distribution, $\sigma(r)$. In the model proposed by Shi and Puls [6], $\sigma(r)$ was set as a constant value equaling σ_p, and r_p was calculated according to a first-order estimate of plastic zone size [9]; as for r_M, it was assumed as 2δ, where δ was the crack opening displacement (COD) and was calculated based on the solution given by Rice and Johnson [10]. Although in the model by Wappling et al. [7], the assumption of $r_M = 2\delta$ and $\sigma(r_M) = \sigma_p$ maintained, $\sigma(r)$ inside the zone $r < r_M$ was set as yield strength of Zircaloy and δ was calculated using the strip-yield model [9]. Kim et al. [8] proposed another model using a cohesive zone model in the plastic zone, with the cohesive stress being zero at the crack tip considering occurrence of damage and σ_p at the boundary of cohesive zone; besides, the cohesive stresses are set to linearly increase from zero to the maximum stress and then decrease to σ_p at the boundary of plastic zone. Shmakov et al. [5] simplified Kim's model by assuming a continuity of the derivative $\frac{d\sigma(r)}{dr}$ at r_p, and obtained that $\sigma_M = \frac{4}{3}\sigma_p, r_M = \frac{1}{3}r_p$.

In most of the current models forK_{IH}, the lengths of plastic zone or cohesive zone were all calculated using a first-order estimate of plastic zone size [9]. In fact, the stresses along the cracking plane are redistributed because of plastic deformation and damage accumulation surrounding the crack tip, so the length of plastic zone should be recalculated, and must increase in size according to the fact that the normal stresses should satisfy equilibrium according to the fracture mechanics theory [9]. If strain hardening is neglected, a simple force balance results in a second-order estimate of plastic zone size which is twice as large as the first-order estimate of plastic zone size by the Irwin approach [9]. If the strain-hardening plastic behavior of Zircaloy is considered, a maximum normal stress larger than σ_p occurs in the plastic zone, and damages will accumulate and lead to a lowered stress at the crack tip. Besides, according to the cohesive zone model, the lowered stress at the crack tip is uneasy to reach zero for the ductile Zircaloy under the threshold stress intensity factor to trigger DHC. Therefore, it is necessary to give a more reasonable distribution of normal stresses in the plastic zone, with the strain-hardening plastic behavior and damage accumulation effect involved.

In the in-pile operation environment, nonhomogeneous temperature variations exist in the cladding tubes, and the constraint conditions will affect the magnitudes of thermal stresses. As a result, the effect of the induced thermal stresses on DHC should be investigated [11] in order to evaluate the safety and optimize the constraint design of fuel rods. Experiments have shown that the plane stress state and plane strain state can have different effects on the DHC velocity [12]. The thermal stresses due to nonhomogeneous temperature variations will change the stress state in the plastic zone, however, studies of these effects on K_{IH} are limited in previous researches, especially for the radial cracking cases.

In this study, according to the fracture mechanics theory of second-order estimate of plastic zone size [9], a new stress distribution is proposed with thermal stress contribution involved for the strain-hardening plastic materials, mainly for the plane-strain state cases such as the radial cracking case. The corresponding theoretical models for threshold stress intensity factor and critical hydride length are developed. Some experimental results of threshold stress intensity factor and critical hydride length for Zircaloy-2 tubes are compared with the theoretical predictions. The effects of thermal stresses on the threshold stress intensity factor and critical hydride length are investigated. Besides, the effects of mechanical properties are discussed, including the yield strength and fracture toughness of Zircaloy together with the fracture strength of hydrided Zircaloy.

2. Theoretical models for threshold stress intensity factor and critical hydride length

As mentioned before, DHC is a repeated multi-field coupling process: the diffusion and accumulation of hydrogen atoms; the precipitation, growth and fracture of hydride when the applied stress intensity factor K_I exceeds the threshold stress intensity factor K_{IH}. Hydrogen atoms will diffuse to the crack tip zone driven by concentration gradient of hydrogen, the gradient of hydrostatic stress and temperature gradient. As shown in Fig. 1, it is supposed that the hydride will firstly precipitate at the location $r = r_M$ where the maximum normal stress perpendicular to the crack plane is reached, and grow along the crack extension line until the critical hydride length l_C is finally attained.

If there are no external loads, the hydride formed ahead of the crack tip is expected to be compressed due to a large (17%) volume increase associated with the transformation from zirconium alloy to brittle hydride [5]. The normal stresses in the plastic zone are generally supposed to be the sum of external-load induced stresses without considering hydride precipitation and the stresses only caused by the hydride formation. As shown in Fig. 1, the maximum normal stress (σ_{22}) is supposed to appear at the point $r = r_M$.

When $K_I = K_{IH}$, the normal stress at r_M reaches the fracture strength of hydrided Zircaloy and the hydride length is assumed to be infinite. Therefore, a local fracture criterion for the hydrided Zircaloy can be described as

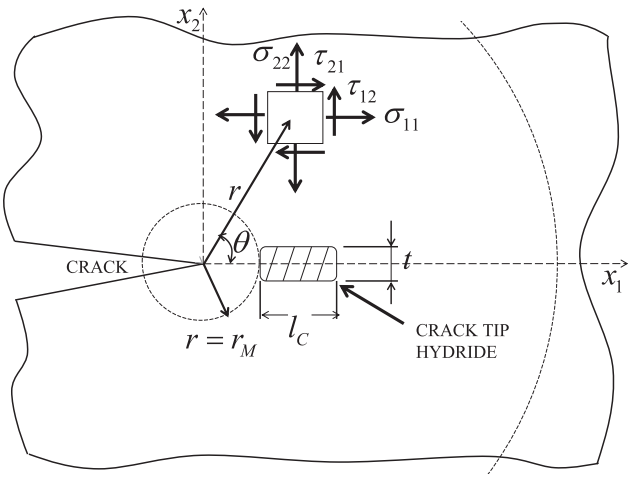

Fig. 1. The schematic diagram for the variables in DHC model.

$$\sigma_{22}(r_M) + \sigma^h(r_M) = \sigma_F \tag{2}$$

where $\sigma_{22}(r)$ is the normal stress induced by external loads when there is no hydride present, $\sigma^h(r_M)$ depicts the normal stresses resulting from the precipitation of infinite length of hydride, which is obtained as [6]

$$\sigma^h(r_M) = -\frac{E\varepsilon_\perp t}{4\pi(1-\nu^2)}\frac{1}{r_M} \tag{3}$$

where E, ν depict the elastic modulus and the Poisson's ratio; $\varepsilon_\perp$ is the vertical misfit strain induced by hydride precipitation; t is the hydride thickness and r_M should satisfy $r_M > 0.25t$.

If the condition $r_M > 0.25t$ is not satisfied, another equation for $\sigma^h(r_M)$ is given as [6]

$$\sigma^h(r_M) = -\frac{E\varepsilon_\perp t}{4\pi(1-\nu^2)}\frac{1}{r_M + \Delta t} \tag{4}$$

where $\Delta = \frac{1}{2\pi}\exp(-6.158 r_M/t)$.

The maximum normal stress σ_M and the distance r_M depend on the stress distribution ahead of the crack tip. In the following, new stress distribution is proposed considering the fracture mechanics theory of the second-order estimate of plastic zone size [9] together with the contribution of thermal stresses.

2.1. The redistributed tensile stresses in the plastic zone

As shown in Fig. 2, there is a long and shallow axial crack AO in the cladding tube, and the crack will propagate in the radial direction under large hoop stresses; local rectangular and cylindrical coordinates at the crack tip are also given. As is known, in the reactor environment there is a temperature gradient between the inside and outside of the tube. When r is small, the temperature distribution along Ox_1 can be expressed as [13]

$$T(r) = Ar^{0.5} + B \tag{5}$$

where A is a coefficient depending on the temperature gradient along the radial direction; B is the temperature at the crack tip.

According to linear elastic fracture mechanics, under plane strain conditions the stress field in the near-tip region is given as

$$\begin{aligned}
\sigma_{11} &= \sigma_{22} = \frac{K_\mathrm{I}}{\sqrt{2\pi r}} \\
\sigma_{33} &= \nu(\sigma_{11} + \sigma_{22}) - \alpha^T E \Delta T \\
\tau_{12} &= \tau_{23} = \tau_{13} = 0
\end{aligned} \tag{6}$$

where $K_\mathrm{I} = K_\mathrm{I}^\sigma + K_\mathrm{I}^\mathrm{T}$, K_I^σ is the mechanical stress intensity factor induced by the pressure on the inside and outside surfaces of the tube, and K_I^T is thermal stress intensity factor induced by thermal gradient, which is small and ignored in this study. Detailed comparisons of these two stress intensity factors are discussed in Appendix. α^T, E, ν depict the secant coefficient of thermal expansion, the elastic modulus and the Poisson's ratio, respectively; ΔT is the temperature increment, which is expressed as

$$\Delta T = T(r) - T_f = Ar^{0.5} + B - T_f \tag{7}$$

where T_f is the reference temperature, which refers to the thermal-stress-free temperature. Thus, the axial thermal stress can be involved when the thermal strains are constrained due to various mechanisms.

As shown in Eq. (6), there is a stress-field singularity at the crack tip. In fact, the singularity is impossible in real cases, as plastic deformation and damages will appear when the normal stress ahead of the crack tip reaches the maximum normal stress σ_M and subsequently the actual stress at the crack tip will decrease due to damage accumulation. Thus, the normal stresses will be redistributed. Based on the correction of plastic zone size by the Irwin approach [9], the distribution of tensile stresses σ_{22} along the crack tip extension line (Line Or in Fig. 3) is proposed in this study, as shown in Fig. 3. The length of plastic region is denoted as r_p in the crack tip zone which contains damages when $r < r_M$. And a virtual crack tip is assumed at $r = r_M$ in order to solve r_M and the length of plastic zone r_p.The stress σ_0 describes the lowered tensile stress owing to damages in the real crack tip. Because Zircaloy is an elasto-plastic material, the stress at the crack tip can't easily reach zero under the external thermo-mechanical loads. In fact, the large strains at the crack tip cause the crack to blunt, which reduces the stress triaxiality locally and makes $\sigma_{11} = 0$, but σ_{22} is not easy to reach zero [9]. The value of σ_0 will be discussed in the following. In the region $(r > r_p)$ outside the plastic region, the stress calculation obeys the theory of linear elastic fracture mechanics, with the stress at the boundary of plastic zone denoted as σ_p.

Under the applied thermo-mechanical loads, following linear elastic fracture mechanics the stress along Or when $r > r_M$ can be obtained as

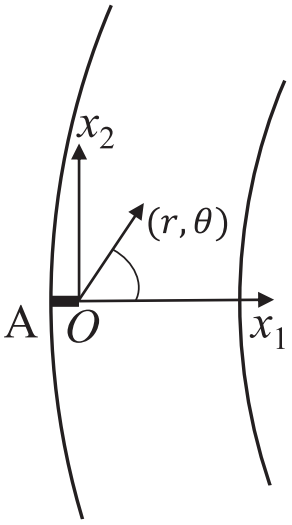

Fig. 2. The cross section of an axially-cracked tube.

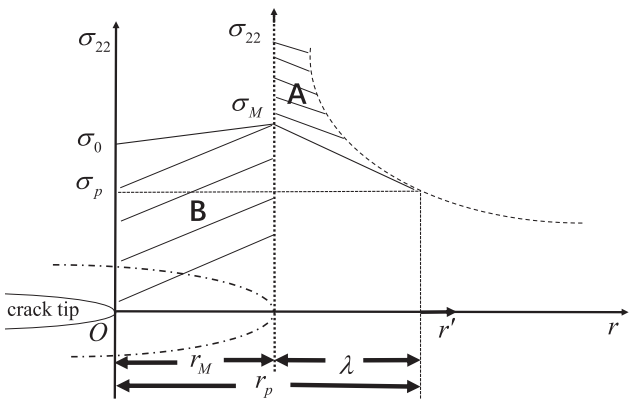

Fig. 3. A schematic diagram of the tensile stresses ahead of the crack tip.

$$\sigma_{11} = \sigma_{22} = \frac{K_I}{\sqrt{2\pi r'}}$$
$$\sigma_{33} = \nu(\sigma_{11} + \sigma_{22}) - \alpha^T E \Delta T \quad (8)$$
$$\tau_{12} = \tau_{23} = \tau_{13} = 0$$

where $r' = r - r_M$, and the plane strain condition is considered. It should be noted that the effect of the virtual crack increment r_M on K_I is ignored.

When $r = r_p$ ($r' = \lambda = r_p - r_M$), the tensile stress σ_{22} in Eq. (8) becomes

$$\sigma_{22}(r_p) = \sigma_p = \frac{K_I}{\sqrt{2\pi\lambda}} \quad (9)$$

By applying Von Mises yield criterion at $r = r_p$, a relation between the plastic zone length and stress intensity factor can be obtained as

$$\sigma_{ys} = (1-2\nu)\frac{K_I}{\sqrt{2\pi\lambda}} + \alpha^T E\left(A\sqrt{r_p} + B - T_f\right) \quad (10)$$

where σ_{ys} is the yield strength.

The force equivalence between redistributed normal stress field in the plastic zone and the local stresses resulting from linear elastic fracture mechanics can be obtained as

$$\frac{\sigma_0 + \sigma_M}{2} r_M + \frac{\sigma_p + \sigma_M}{2}\lambda = \int_0^{\lambda} \frac{K_I}{\sqrt{2\pi\xi}}\, d\xi \quad (11)$$

Combining Eq. (11) with Eq. (9), the position of maximum stress r_M and the length of plastic zone r_p are given as

$$r_M = \frac{3\sigma_p - \sigma_M}{\sigma_M + \sigma_0}\lambda \quad (12)$$

$$r_p = \frac{3\sigma_p + \sigma_0}{\sigma_M + \sigma_0}\lambda \quad (13)$$

It is noted that the value of the maximum stressσ_M depends on the material's deformation characteristics. For a plane strain state, by using the Hutchinson, Rice, Rosengren (HRR) singular solution for strain-hardening materials [14,15], σ_M can be obtained as [16]

$$\sigma_M = \sigma_{22}(r_M) = 3.35\sigma_{ys} \quad (14)$$

The stress σ_0 is expressed as $\sigma_0 = c\sigma_{ys}$. $c = 3.35$ is assumed in this study, and means the normal stress at the crack tip is equal to the maximum stress, believing that the tensile stress at the crack tip is a little lower than the maximum stress for $K_I = K_{IH}$. Besides, in the following sections the results under the assumption $c = 0$ will also be discussed for comparison.

2.2. Threshold stress intensity factor

If $r_M > 0.25t$ is satisfied, from Eqs. (2), (3), (9), (12) and (14), a nonlinear equation that the threshold stress intensity factor satisfies is derived out as

$$\left[3\sigma_p(K_{IH}) - 3.35\sigma_{ys}\right]\left(\frac{K_{IH}}{\sigma_p(K_{IH})}\right)^2 = \frac{(3.35+c)E\varepsilon_\perp t\sigma_{ys}}{2(1-\nu^2)(3.35\sigma_{ys} - \sigma_F)} \quad (15)$$

where K_{IH} can be obtained from this equation using Newton iteration method. σ_p is the normal stress in Eq. (9) as a function of K_I. σ_p can be obtained by combining Eqs. (9), (10), (13) and (14) for a given $K_I = K_{IH}^n$, where K_{IH}^n is the nth iteration value of K_{IH}.

When the temperature gradient is not considered, $\sigma_p(K_{IH})$ can be written as

$$\sigma_p = \frac{\sigma_{ys} - \alpha^T E\left(B - T_f\right)}{1-2\nu} \quad (16)$$

Thus, if $c = 3.35$, Eq. (15) can be expressed as

$$K_{IH} = \frac{\overline{\sigma}_{ys}}{(1-2\nu)}\sqrt{\frac{3.35E\varepsilon_\perp t}{(1-\nu^2)(3.35\sigma_{ys} - \sigma_F)\left(\frac{3x}{1-2\nu} - 3.35\right)}} \quad (17)$$

where $\overline{\sigma}_{ys} = \sigma_{ys} - \alpha^T E(B - T_f)$, $x = \frac{\overline{\sigma}_{ys}}{\sigma_{ys}}$.

If $c = 0$, Eq. (15) can be expressed as

$$K_{IH} = \frac{\overline{\sigma}_{ys}}{(1-2\nu)}\sqrt{\frac{3.35E\varepsilon_\perp t}{2(1-\nu^2)(3.35\sigma_{ys} - \sigma_F)\left(\frac{3x}{1-2\nu} - 3.35\right)}} \quad (18)$$

Therefore, when the temperature gradient is not considered, K_{IH} for $c = 3.35$ is $\sqrt{2}$ times as large as K_{IH} for $c = 0$.

2.3. Critical hydride length

In order to obtain the critical hydride length for a stress intensity factor $K_I > K_{IH}$, based on Ref. [5], a two-phase composite model is adopted to describe the material ahead of the crack tip, as shown in Fig. 4, where $\alpha + \delta$ region contains the plastic α-phase Zircaloy and brittle δ-phase hydride. The degraded fracture toughness of the formed two-phase composite material is assumed to be the weighed superposition of the ones of the two phases. When the applied stress intensity factor K_I equals the degraded fracture toughness, the critical hydride length l_C is reached and fracture will happen, so we have

$$K_I = V_f^\alpha K_I^\alpha + V_f^\delta K_I^\delta = \frac{r_M}{r_M + l_C}K_I^\alpha + \frac{l_C}{r_M + l_C}K_I^\delta \quad (19)$$

where V_f^α and V_f^δ are the volume fractions of α-phase and δ-phase, K_I^α is the fracture toughness of α-phase, K_I^δ represents the fracture toughness for the compressed hydride in the Zircaloy matrix with $K_I^\delta = K_{IH}$. r_M is the position of maximum stress and can be obtained from Section 2.1. Therefore, the equation for l_C is obtained as

$$l_C = \left(\frac{K_I^\alpha - K_I}{K_I - K_{IH}}\right) r_M \quad (20)$$

When the temperature gradient is not considered, Eq. (20) can be simplified as

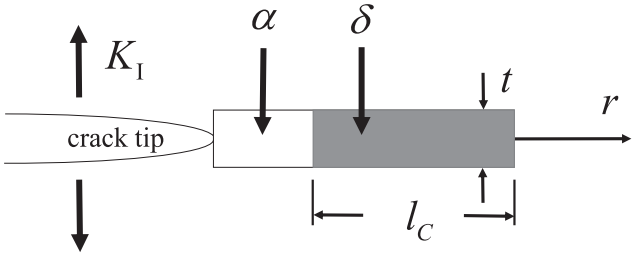

Fig. 4. The precipitated hydride platelet away from the crack tip.

$$l_C = \frac{(3x - 3.35(1-2\nu))(1-2\nu)}{2\pi(3.35+c)x^2}\left(\frac{K_{\mathrm{I}}^{\alpha} - K_{\mathrm{I}}}{K_{\mathrm{I}} - K_{\mathrm{IH}}}\right)\left(\frac{K_{\mathrm{I}}}{\sigma_{ys}}\right)^2 \quad (21)$$

where $x = \frac{\sigma_{ys} - \alpha^T E(B - T_f)}{\sigma_{ys}}$.

3. Validation of the theoretical models

Kubo et al. [3] conducted some experimental tests on the delayed hydride cracking for Zircaloy-2 cladding tubes. Pre-cracks were produced at the outer surface of the tubes, and these cracks propagated in the radial direction to the inner surface under external loads. The material properties of theses tubes are listed in Table 1. In the table, CW refers to the Zircaloy-2 tubes fabricated in the cold worked condition, and SR450 means the Zircaloy-2 tubes annealed at 450°C. Besides, the values of yield strength for CW above 275°C and SR450 above 250°C are extrapolated according to the experimental data in Ref. [3] for the lack of more data. In addition, a constant hydride thickness $t = 2$ μm is used in this model. It should be noted that the vertical misfit strain induced by hydride precipitation and the fracture toughness of Zircaloy are temperature dependent. In these experiments [3], the thermal stresses in the cladding tubes can be neglected according to the designed temperature loading process, especially for the cases of constant temperature DHC tests. Thus, model predictions in this section will not take the thermal stresses into account.

Comparison of threshold stress intensity factor (K_{IH}) calculated by different theoretical models with the experimental data [3] can be found in Fig. 5 for the material of CW. Three sets of theoretical results are obtained by Eq. (17), respectively for $c = 0$, $c = 3.35$ and the case with $c = 3.35$ and enlarged vertical misfit strain induced by hydride precipitation. The theoretical predictions by the other two models [5,6] are also plotted.

Table 1
Parameters of Zircaloy-2 cladding tube materials.

Parameters	Material models and variable values	Ref.
σ_{ys}(CW)	$1307 - 1.369T$ MPa	[3]
σ_{ys}(SR450)	$828.89 - 1.1556(T - 273)$ MPa	[3]
ν	$0.3908 - 8\times10^{-5}T$	[3]
E	$115.39 - 0.0634T$ GPa	[3]
σ_F	$676 - 0.09T$ MPa	[17]
$\varepsilon_\perp$	$0.06646 + 1.9348\times10^{-5}T$	[18]
$\varepsilon^{th} = \alpha^T(T - T_f)$	$-1.238\times10^{-3} + 4.441\times10^{-6}T$, 300 K $< T <$ 1073 K, $T_f = 300$ K	[19]
K_f^{α}	$30 + 0.045(T - 300)$ MPa$\sqrt{\mathrm{m}}$	[7]

(T is the temperature in Kelvin).

The model predictions in this study indicate that K_{IH} decreases with the temperature in the given range. It is obvious that K_{IH} for $c = 3.35$ is greater than that for $c = 0$. One can see that the theoretical results for $c = 3.35$ have a good agreement with the experimental ones. So the assumption of $c = 3.35$ in the developed model of this study is suitable, and the developed model can be validated. The predictions from the theoretical model in Ref. [6] underestimate the threshold stress strength factors largely. While, the threshold stress strength factors are overestimated by the model in Ref. [5]. And it should be noted that $r_M > 0.25t$ is satisfied in all the calculations, and the models for the hydride thickness and vertical misfit strain $\varepsilon_\perp$ in Refs. [5,6] are adopted to obtain the results for model predictions [5] and [6] in Fig. 5. In order to investigate the effects of vertical misfit strain, the model predictions with a higher strain magnitudes denoted as $1.2\varepsilon_\perp$ are also given in Fig. 5. It can be seen that a higher $\varepsilon_\perp$ could make K_{IH} larger, and the corresponding theoretical results seem to match the experimental ones better. So, the misfit strains due to hydride precipitation can have a certain effect on the threshold stress intensity factor.

According to the experimental measurement after testing at 200°C in Ref. [3], the length of radial hydrides for SR450 tubes was found to be from about 14 μm to 18 μm. Fig. 6 gives the critical hydride length for different stress intensity factors at 200°C together with the position of maximum stress r_M. It can be seen that l_C decreases with K_{I} ($K_{\mathrm{I}} > K_{\mathrm{IH}}$), and it approaches infinity when K_{I} is close to K_{IH}. l_C is predicted to be about 20 μm when K_{I} is 10 MPa$\sqrt{\mathrm{m}}$ which is close to the experimental condition [3], which is consistent with the experimental measurement of 18 μm. While, the prediction of l_C by the model in Ref. [5] is about half as large as the model predictions in this study. Therefore, the model for the critical hydride length has been improved to some extent, and the difference between the predicted results and the experimental ones may result from and the uncertainties of material yield strength and fracture toughness at 200°C. In Ref. [3], only the values of yield strength at 25°C and 250°C for SR450 were given. The yield strength at 200°C is obtained according to the fitting relation as a

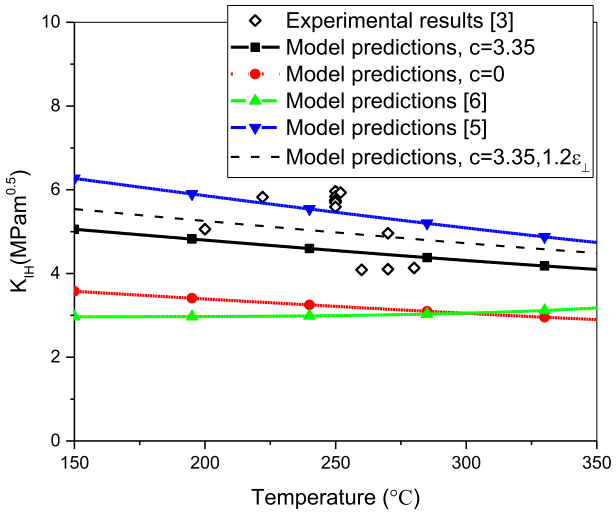

Fig. 5. Comparison of the predicted threshold stress intensity factors between model predictions and experimental results.

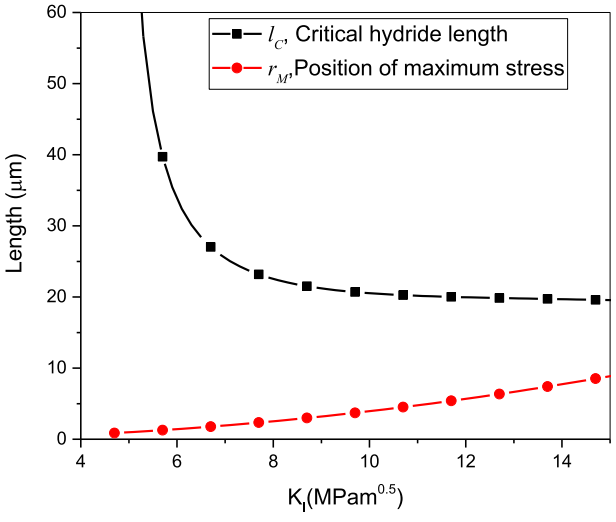

Fig. 6. The critical hydride length and position of maximum stress for different stress intensity factors.

function of temperature. The position of maximum stress away from the crack tip r_M rises as K_I increases, and is greater than 0.25t, so, Eqs. (17) and (21) are effective under most conditions.

4. Results and discussions

4.1. Effects of thermal stress

According to Eq. (7), when the reference temperature equals the temperature at the crack tip, the axial thermal stresses can be induced by temperature gradients. When the temperature gradient is not zero, there is no explicit formula to calculate the threshold stress intensity factor, and the Newton iterative method is adopted to solve K_{IH} with only several iterations to obtain the convergent results. As Eq. (5) is used to describe the temperature distribution, A is related with temperature gradient, so different values of A are considered to investigate the effect of temperature gradient, as is shown in Fig. 7. A higher value of A means a higher temperature gradient [20]. One can see that a positive temperature gradient makes K_{IH} smaller, while a negative temperature gradient makes it larger, but they have a very small impact on K_{IH}. Therefore, the effects of temperature gradient are very slight and can be ignored.

The reference temperature can lead to a temperature change, which can induce thermal stresses. The effects of reference temperature on the threshold stress intensity factor are shown in Fig. 8, where B is the temperature at the crack tip and T_f is the reference temperature. It is noted that the reference temperature refers to the temperature resulting in no thermal stresses, and after that the thermal expansion or shrinkage is constrained to cause thermal stresses. The case with $T_f = B$ means thermal stresses are not considered. It can be seen that if the reference temperature is 300 K, K_{IH} will be smaller compared to the case with $T_f = B$. In the in-pile operation environment, the temperatures of cladding tubes are higher than room temperature. If the axial deformation is constrained, the axial thermal stresses could exist, making K_{IH} lower. In order to raise K_{IH} for cladding tubes, the axial thermal stress should be avoided, for example, by weakening the constraint in the axial direction. In the DHC experiments, the specimens are usually heated to a certain temperature and kept for some time, which is followed by lowering the temperature to the test temperature. As can be seen from the results with T_f = 608 K, if the shrinkage deformation during the course of decreasing temperature is constrained, the reference temperature should be higher than the test

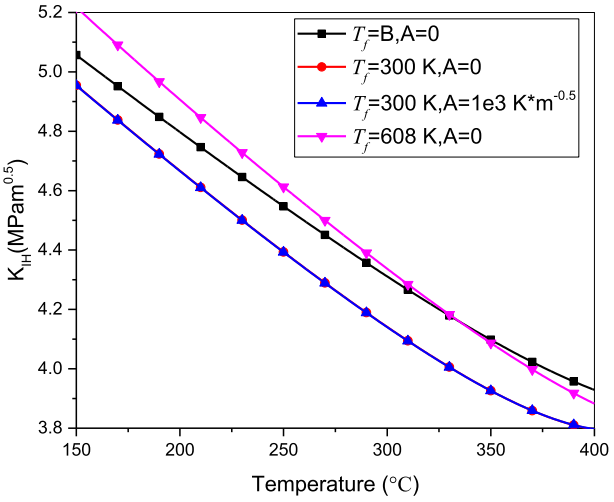

Fig. 8. Effects of reference temperature on K_{IH}.

temperature, which will make K_{IH} higher than the case no thermal stress is considered. One can also see that the effect of temperature gradient on K_{IH} is much smaller than that of reference temperature.

As mentioned before, the critical hydride length, l_C, decreases with increasing the stress intensity factor K_I. Fig. 9 displays the relation between l_C and K_I at different temperatures. It is evident that l_C is larger at a higher temperature when K_I is greater than 6 MPa$\sqrt{m}$. Besides, when K_I is in the range from 9 MPa$\sqrt{m}$ to 15 MPa$\sqrt{m}$, l_C changes slowly, so it can explain, to some extent, the phenomenon that the DHC velocity changes gradually at a certain range of K_I.

The critical hydride length can be also affected by thermal stresses. As shown in Fig. 10, the critical hydride length, l_C, increases with the temperature, and the results are obtained for a stress intensity factor of 12 MPa$\sqrt{m}$. Fig. 10 also gives the results at different temperature gradients. One can see that l_C increases with the temperature, at 400°C it is more than four times as long as that at 150°C. It can be found that the effect of temperature gradient can be neglected.

Fig. 11 shows the effects of reference temperature on the critical hydride length. One can see that if the reference temperature is lower than the temperature at the crack tip, l_C will increase by

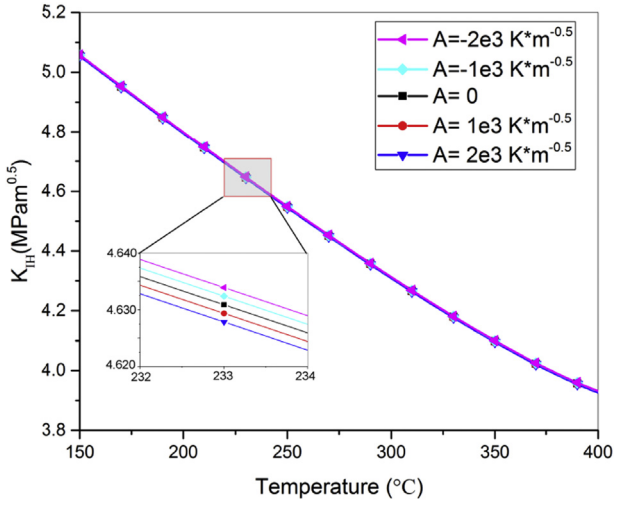

Fig. 7. Effect of temperature gradients on K_{IH}.

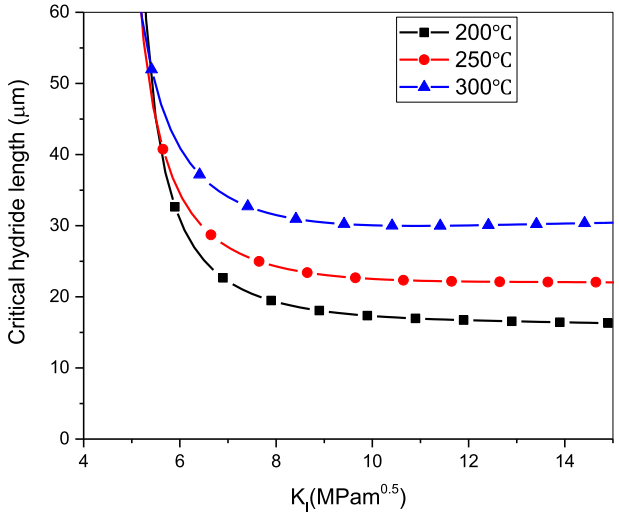

Fig. 9. Relation between the critical hydride length and K_I at different temperatures.

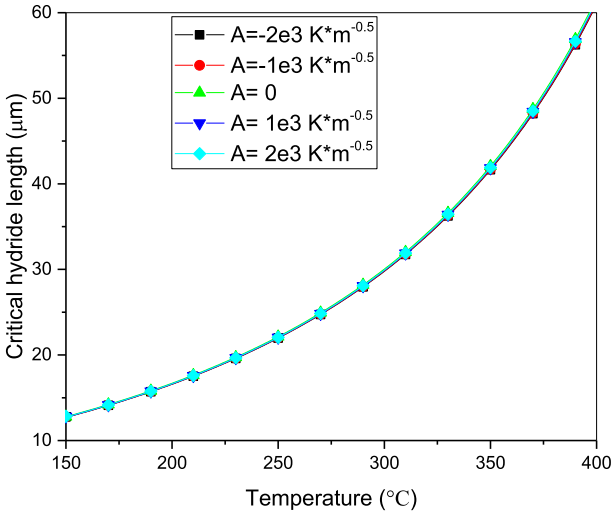

Fig. 10. Effects of temperature gradient on critical hydride length.

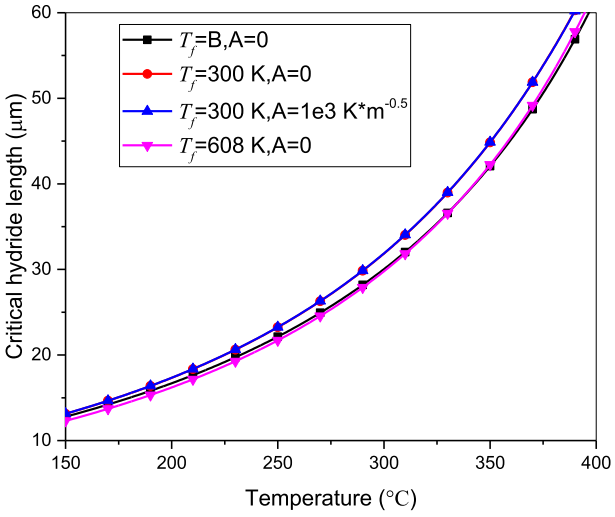

Fig. 11. Effects of reference temperature on critical hydride length.

2.6%–6.6% compared to the case no thermal stress is considered. If the reference temperature is higher than the test temperature (the temperature at the crack tip), l_C will be smaller, which implies that the DHC velocity may be higher as it may take less time to form enough length of hydride. In Ref. [3], it was mentioned that the DHC velocity results are somewhat faster for the decreasing temperature tests than those for the constant temperature tests. In the decreasing temperature tests, the test temperature was decreasing when applying the tensile loads. For the reason that the loading device intimately contacted with the cladding tube when decreasing the test temperature, the shrinkage deformation is constrained resulting in large axial tensile stresses, which is equivalent to the case with a high reference temperature than the test temperature. One can conclude that the DHC velocity might be smaller in the nuclear reactors if the axial deformation of the cladding tubes is constrained although the threshold stress intensity factor is reduced. However, in the transient operation condition such as a rapid power ramp, the effects of thermal stresses will be of complexity.

4.2. Effects of mechanical properties

There are many factors that affect threshold stress intensity factor and critical hydride length such as the crystallographic texture of the cladding and irradiation effects. The texture of zirconium grains have been found to have a significant influence on the threshold stress intensity factor [2,21]. It's been shown that radially-oriented hydrides are much more detrimental to mechanical properties than circumferentially-oriented hydrides [22]. The mechanical strength of Zircaloy can also be significantly affected by the formation of hydride [23]. Irradiation can also exert an effect on the mechanical properties due to irradiation hardening and irradiation embrittlement. In the following, the effects of mechanical properties on threshold stress intensity factor and critical hydride length will be discussed, and thermal stress is not considered in these calculations.

The threshold stress intensity factor at 250°C is plotted versus yield strength in Fig. 12. It can be seen that the model predictions of K_{IH} in this study indicates that it will decrease to a minimum value and then increase with the yield strength. Model predictions by Ref. [5] show that K_{IH} will have a rise with increasing yield strength. While, the model predictions by Ref. [6] reveal that K_{IH} will decrease with increasing yield strength. The experimental results in Ref. [3] demonstrate that K_{IH} has a trend to firstly decrease then increase with the yield strength, which reflects a consistent trend with the model predictions in this study. As mentioned previously, a higher $\varepsilon_\perp$ could make K_{IH} higher, the model predictions with higher $\varepsilon_\perp$ seem to have a better agreement with the experimental ones. According to Eq. (17), yield strength should be greater than $\frac{1}{3.35}\sigma_F$ to get an effective K_{IH}, otherwise DHC will not take place. It can be found from Eq. (19) that the minimum value of K_{IH} will be reached when yield strength is $\frac{2}{3.35}\sigma_F$, so the model predictions by the theoretical model in this study present a variation rule depicted in Fig. 12. It should be noted that $r_M > 0.25t$ is satisfied in the current calculations, otherwise Eq. (4) should be considered, which may happen when yield strength is much larger.

The yield strength of zircaloy could also affect the critical hydride length, as depicted in Fig. 13. The considered stress intensity factor, K_I, is 12 MPa$\sqrt{m}$. It is evident that smaller yield strength can lead to a larger value of critical hydride length, which can be also obtained from Eq. (21). Besides, the values of fracture toughness for different Zircaloy materials also have uncertainties. According to Eq. (21), a smaller fracture toughness of Zircaloy can reduce the critical hydride length, as displayed in Fig. 14. Due to the increase in yield strength induced by irradiation hardening and the decrease in

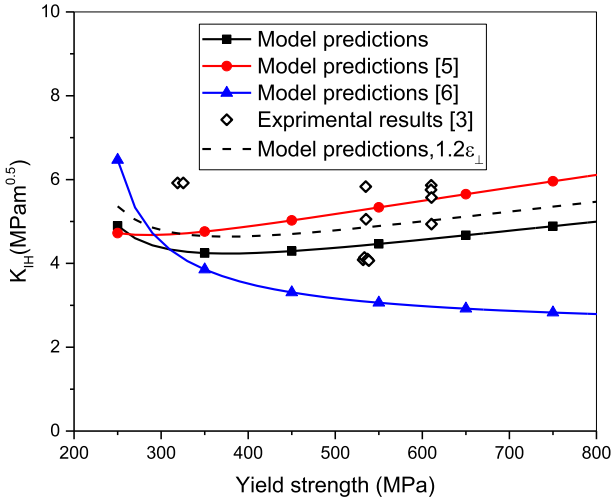

Fig. 12. The effects of yield strength on K_{IH}.

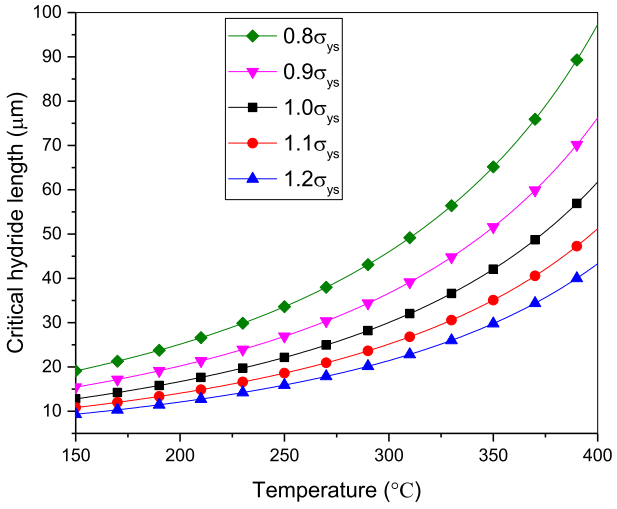

Fig. 13. The effects of yield strength on critical hydride length.

fracture toughness induced by irradiation embrittlement, there will be a smaller critical hydride length if irradiation effect is involved. It can be obtained that the DHC velocity in the steady crack growth stage will be faster for the irradiated Zircaloy tubes although the threshold stress intensity factor is heightened.

According to Eq. (17), a larger fracture strength of hydrided Zircaloy can make K_{IH} larger as it is much more difficult to fracture with a higher fracture strength. The sensitivity analysis is also performed for the fracture strength of hydrided Zircaloy. By magnifying the fracture strength σ_F by a factor larger than 1.0, the obtained results can be found in Fig. 15. One can see that, K_{IH} will increase with the fracture strength σ_F; when the values of σ_F are less than 1.5 times of the initial values at different temperatures, K_{IH} have a trend of decreasing with an increase of temperature; while when the values of σ_F are twice as large as its initial values, K_{IH} will firstly increase very slowly with the temperature, and at higher temperatures K_{IH} will be very sensitive to the temperature increase. It was also reported in the experiments by Holston et al. [24] that K_{IH} could be enlarged as temperature increases. Therefore, DHC is difficult to occur at high temperatures when σ_F is comparably large. From Eq. (19), one can find that the factor $(3.35\sigma_{ys} - \sigma_F)$ in the denominator can affect the magnitude of K_{IH} remarkably. If it is

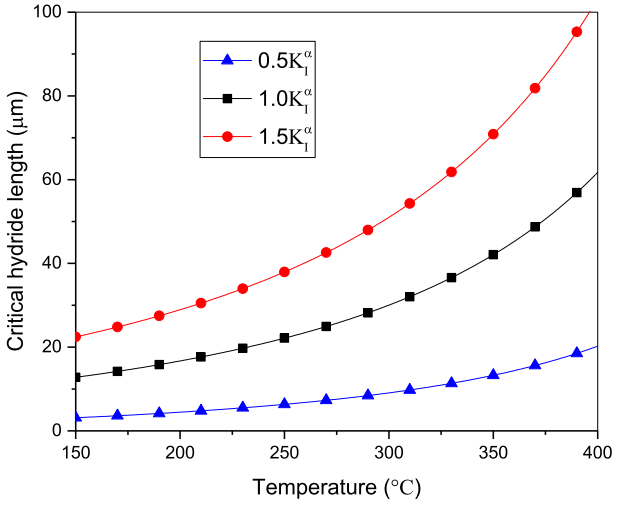

Fig. 14. The effects of fracture toughness of zircaloy on critical hydride length.

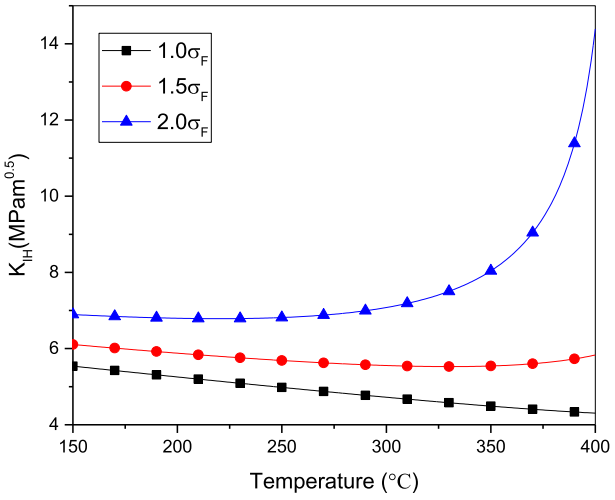

Fig. 15. Effects of fracture strength of hydride on K_{IH}.

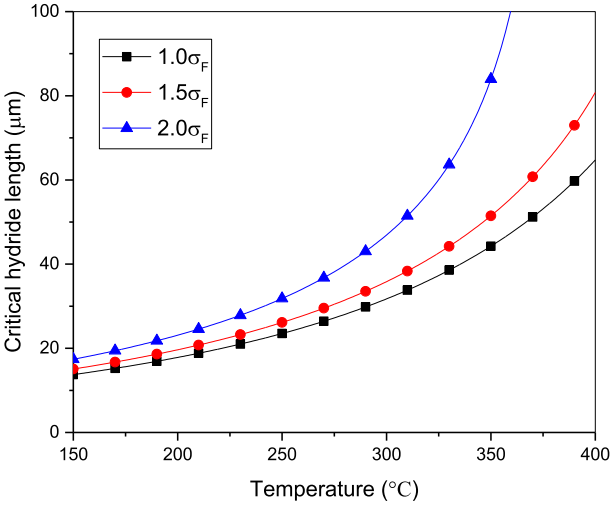

Fig. 16. Effects of fracture strength of hydride on critical hydride length.

very small and larger than zero, it will lead to a high value of K_{IH}. With increasing the temperature, the yield strength of Zircaloy materials tends to decrease, the factor $(3.35\sigma_{ys} - \sigma_F)$ might be very small or less than zero for some cases, so that the DHC can be arrested at high temperatures for a certain stress intensity factor. This might be an important mechanism of crack arrest at higher temperatures for some Zircaloy materials. The actual behavior depends on the values of yield strength and fracture strength for hydrided Zircaloy at higher temperatures.

Fracture strength σ_F could also affect the critical hydride length, as illustrated in Fig. 16. It can be seen that a higher σ_F can make l_C larger. The values of l_C are all calculated with K_I equaling 12 MPa$\sqrt{m}$ which is very close to K_{IH} at high temperatures under a large fracture strength, so l_C is very large at these conditions implying that DHC may not occur. And it is consistent with the phenomenon that there is usually a crack arrest temperature above which DHC velocity is so small that DHC does not occur.

5. Conclusions

A new stress distribution in the plastic zone with thermal stresses considered is derived based on a second-order estimate of

plastic zone size, and new theoretical models to calculate threshold stress intensity factor and critical hydride length are given in this study. A good agreement of model predictions with the experimental results is obtained. As the temperature gradient exerts little effect on K_{IH} and l_C for the radial cracking cases, the effect of temperature gradient can be ignored and the models can be simplified as Eq. (17) and Eq. (21) with $c = 3.35$. The effects of thermal stresses and mechanical properties are also discussed, and conclusions can be drawn as follows.

(1) A larger positive change of temperature can make K_{IH} smaller and l_C larger. The effects of thermal stresses should be considered in the safety evaluation and optimized constraint design for fuel rods in the nuclear reactors.
(2) The critical hydride length l_C change slightly when the stress intensity factor is in a certain range for Zircaloy materials, and it increases with temperature in this range.
(3) An increase in yield strength of zircaloy will result in a decrease in the critical hydride length l_C, and K_{IH} will firstly decrease and then have a trend to increase with the yield strength of Zircaloy. l_C also increases with the fracture toughness. Irradiated Zircaloy tubes will have a higher threshold stress intensity factor and faster DHC velocity.
(4) A large fracture strength of hydrided Zircaloy could make K_{IH} and l_C extremely large at high temperatures, making DHC difficult to happen, which mainly results from the very small or negative values of $(3.35\sigma_{ys} - \sigma_F)$ in Eq. (19).

Acknowledgement

The authors thank for the supports of National Natural Science Foundation of China (No. 11772095, 11572091), the support of the National Key Research and Development Program of China (No. 2016YFB0700103) and the supports of the foundation from Science and Technology on Reactor System Design Technology Laboratory.

Appendix. Comparison between mechanical stress intensity factor and thermal stress intensity factor for the in-plane stresses

As it is difficult to obtain the stress intensity factors for tubes with edge cracks, the formulae for an infinite plate with a central crack are used to estimate these stress intensity factors. The crack has a length of $2a$ with a uniform tensile stress σ^{∞} perpendicular to crack plane at infinite and a temperature gradient component k along crack plane at infinite position. The Mode I singular field can be determined by the stress intensity factor, K_I, which consists of mechanical stress intensify factor and thermal stress intensity factor.

The mechanical stress intensify factor is

$$K_I^{\sigma} = \sigma^{\infty}\sqrt{\pi a} \tag{A.1}$$

For a plane strain condition, the thermal stress intensity factor given by Tang [20] is expressed as

$$K_I^{T} = \frac{\alpha^T E a k}{4-4\nu}\sqrt{\pi a} \tag{A.2}$$

When the temperature gradient is 50 K/mm and the temperature is 523 K, with the material properties in Table 1 used, the comparison between the obtained two stress intensity factors are shown in Table 2. The results are displayed at different tensile stresses and crack lengths, and small values of crack lengths are used due to that many cladding tubes have a wall thickness of 0.7 mm. One can see that thermal stress intensity factor is quite small compared to mechanical stress intensity factor, thus, the thermal stress intensity factor can be ignored in the theoretical models for the threshold stress intensity factor and critical hydride length, which means K_I^T is ignored in Eq. (8). However, it should be noted that the thermal stress component in x_3 direction can still contribute to the threshold stress intensity factor and critical hydride length for DHC, which results from displacement constraint in the axial direction of cladding tubes.

Table 2
Comparison between mechanical stress intensify factor and thermal stress intensify factor.

σ^{∞} (MPa)	a(μm)	K_I^{σ} (MPa$\sqrt{\text{m}}$)	K_I^{T} (MPa$\sqrt{\text{m}}$)	$\frac{K_I^T}{K_I^{\sigma}} \times 100\%$
300	50	3.760	0.005	0.128
	200	7.520	0.039	0.512
	300	9.210	0.071	0.768
400	50	5.013	0.005	0.096
	200	10.027	0.039	0.384
	300	12.280	0.071	0.576
500	50	6.267	0.005	0.077
	200	12.533	0.039	0.307
	300	15.350	0.071	0.461

References

[1] M.P. Puls, The Effect of Hydrogen and Hydrides on the Integrity of Zirconium Alloy Components: Delayed Hydride Cracking, Springer, London, 2012.
[2] K.S. Chan, An assessment of delayed hydride cracking in zirconium alloy cladding tubes under stress transients, Int. Mater. Rev. 58 (2013) 349–373.
[3] T. Kubo, Y. Kobayashi, H. Uchikoshi, Measurements of delayed hydride cracking propagation rate in the radial direction of Zircaloy-2 cladding tubes, J. Nucl. Mater. 427 (2012) 18–29.
[4] S. Shimada, E. Etoh, H. Hayashi, Y. Tukuta, A metallographic and fractographic study of outside-in cracking caused by power ramp tests, J. Nucl. Mater. 327 (2004) 97–113.
[5] A.A. Shmakov, R.N. Singh, D. Yan, R.L. Eadie, Y.G. Matvienko, A combined SIF and temperature model of delayed hydride cracking in zirconium materials, Comput. Mater. Sci. 39 (2007) 237–241.
[6] S.Q. Shi, M.P. Puls, Criteria for fracture initiation at hydrides in zirconium alloys I. Sharp crack tip, J. Nucl. Mater. 208 (1994) 232–242.
[7] D. Wappling, A.R. Massih, P. Stahle, A model for hydride-induced embrittlement in zirconium-based alloys, J. Nucl. Mater. 249 (1997) 231–238.
[8] Y.S. Kim, Y.G. Matvienko, Y.M. Cheong, S.S. Kim, S.C. Kwon, A model of the threshold stress intensity factor, KIH, for delayed hydride cracking of Zr–2.5Nb alloy, J. Nucl. Mater. 278 (2000) 251–257.
[9] T.L. Anderson, Fracture Mechanics: Fundamentals and Applications, third ed.ed, Taylor & Francis/CRC Press, Boca Raton, FL, 2005.
[10] J.R. Rice, M.A. Johnson, The Role of Large Crack Tip Geometry Changes in Plane Strain Fracture, Inelastic Behavior of Solids, 1970, pp. 641–672.
[11] S. Sagat, C.K. Chow, M.P. Puls, C.E. Coleman, Delayed hydride cracking in zirconium alloys in a temperature gradient, J. Nucl. Mater. 279 (2000) 107–117.
[12] S. Sunil, A.K. Bind, H.K. Khandelwal, R.N. Singh, J.K. Chakravartty, Effect of specimen thickness on DHC velocity for Zr-2.5Nb alloy pressure tube material, J. Nucl. Mater. 467 (2015) 373–382.
[13] G.C. Sih, On the singular character of thermal stresses near a crack tip, J. Appl. Mech. 29 (1962) 587–589.
[14] J.W. Hutchinson, Singular behaviour at the end of a tensile crack in a hardening material, J. Mech. Phys. Solid. 16 (1968) 13–31.
[15] J.R. Rice, G.F. Rosengren, Plane strain deformation near a crack tip in a power-law hardening material, J. Mech. Phys. Solid. 16 (1968) 1–12.
[16] M.P. Puls, Effects of crack tip stress states and hydride-matrix interaction stresses on delayed hydride cracking, Metall. Trans. A 21 (1990) 2905–2917.
[17] S.Q. Shi, M.P. Puls, Fracture strength of hydride precipitates in Zr–2.5Nb alloys, J. Nucl. Mater. 275 (1999) 312–317.
[18] R.N. Singh, P. Ståhle, A.R. Massih, A.A. Shmakov, Temperature dependence of misfit strains of δ-hydrides of zirconium, J. Alloy Compd. 436 (2007) 150–154.
[19] D.L. Hagrman, G.A. Reymann, MATPRO-version 11: a Handbook of Materials Properties for Use in the Analysis of Light Water Reactor Fuel Rod Behavior, Specific Nuclear Reactors & Associated Plants, 1979.
[20] X.S. Tang, Mechanical/thermal stress intensification for mode I crack tip: fracture initiation behavior of steel, aluminum and titanium alloys, Theor. Appl. Fract. Mech. 50 (2008) 92–104.
[21] Y.S. Kim, S.S. Kim, S.C. Kwon, Y.M. Cheong, K.S. Im, Anisotropic threshold stress intensity factor, KIH and crack growth rate in delayed hydride cracking of Zr-2.5Nb pressure tubes, Metall. Mater. Trans. A 33 (2002) 919–925.

[22] J. Bair, M. Asle Zaeem, M. Tonks, A review on hydride precipitation in zirconium alloys, J. Nucl. Mater. 466 (2015) 12–20.
[23] T. Kubo, Y. Kobayashi, H. Uchikoshi, Determination of fracture strength of δ-zirconium hydrides embedded in zirconium matrix at high temperatures, J. Nucl. Mater. 435 (2013) 222–230.
[24] A. Alvarez Holston, J. Stjärnsäter, On the effect of temperature on the threshold stress intensity factor of delayed hydride cracking in light water reactor fuel cladding, Nucl. Eng. Technol. 49 (2017) 663–667.